

Iterative structural identification framework for evaluation of existing structures

Romain Pasquier^{a,*}, Ian F. C. Smith^a

^a*Applied Computing and Mechanics Laboratory (IMAC), School of Architecture, Civil and Environmental Engineering (ENAC), Swiss Federal Institute of Technology (EPFL), CH-1015 Lausanne, Switzerland*

Abstract

Evaluation of aging infrastructure has been a world-wide concern for decades due to its economic, ecological and societal importance. Existing structures usually have large amounts of unknown reserve capacity that may be evaluated through structural identification in order to avoid unnecessary expenses related to the repair, retrofit and replacement. However, current structural identification techniques that take advantage of measurement data to infer unknown properties of physics-based models fail to provide robust strategies to accommodate systematic errors that are induced by model simplifications and omissions. In addition, behavior diagnosis is an ill-defined task that requires iterative acquisition of knowledge necessary for exploring possible model classes of behaviors. This aspect is also lacking in current structural identification frameworks. This paper proposes a new iterative framework for structural identification of complex aging structures based on model falsification and knowledge-based reasoning. This approach is suitable for ill-defined tasks such as structural identification where information is obtained gradually through data interpretation and in-situ inspection. The study of a full-scale existing bridge in Wayne, New Jersey (USA) confirms that this framework is able to support structural identification through combining engineering judgment with on-site measurements and is robust with respect to effects of systematic uncertainties. In addition, it is shown that the iterative structural-identification framework is able to explore the compatibility of several model classes by model-class falsification, thereby helping to provide robust diagnosis and prognosis.

Keywords: Systematic errors, model falsification, knowledge-based reasoning, model-class exploration, behavior diagnosis, prognosis

1. Introduction

Due to conservative strategies that are fueled by high risks associated with the construction of large civil structures, most structures today have significant amounts of unknown reserve capacity. In the context of

*Corresponding author. Address: EPFL ENAC IIC IMAC, Station 18, CH-1015 Lausanne, Switzerland. Phone number: +41 21 693 2498

Email address: rpasquie@gmail.com (Romain Pasquier)

4 structural health management of existing aging structures, structural identification is attractive for decision-
5 making support. The goal of model-based data interpretation is to increase the knowledge of real behavior of
6 complex structures using information provided by behavior measurements. In order to interpret measurement
7 data, physics-based models are used to connect hypotheses of structural behavior to observed behavior
8 and to identify uncertain parameter values of physical properties. This interpretation serves to improve
9 behavior diagnosis and reduce uncertainties associated with behavior prognoses, such as remaining-fatigue-
10 life evaluation. However, diagnosis is an ill-defined task that is performed under conditions of high modeling
11 and measurement uncertainty. In addition, modeling errors are usually systematic, also called epistemic
12 errors as opposed to random errors, thereby increasing interpretation difficulty.

13 Single-model-updating approaches such as residual minimization have already shown to be inaccurate in
14 the presence of systematic errors since a single optimal model is intrinsically imperfect due to parameter-value
15 compensation [1–4]. Instead, there are always multiple models that are able to explain observations of the
16 behavior of complex structures. Approaches such as probabilistic Bayesian inference accounts for multiple
17 solutions through updating posterior probabilities of parameter values, thereby estimating the uncertainty
18 associated with the parameter values. However, a common assumption in these approaches is that modeling
19 and measurement errors are adequately described by a joint independent zero-mean Gaussian probability
20 density function (PDF) [5–7], which is incompatible with the systematic nature of several modeling uncer-
21 tainty sources. In addition, some applications incorporate the variance of the joint PDF as a parameter
22 in the identification process [8–10] and others assign an arbitrary value to the variance [11–13]. However,
23 in complex civil structures, modeling uncertainties are often biased and correlated spatially. In addition,
24 defining a statistical model of errors that is not compatible with the true errors leads to biased diagnostics
25 and prognosis [3, 14]. While Bayesian inference may provide useful support when statistical model of errors
26 is known, it is not robust when aspects such as correlations cannot be quantified.

27 For the purposes of this paper a model class is defined as a parameterized physics-based model, where
28 parameters are variables whose values need to be identified. Models are instances of model classes. In
29 the context of Bayesian inference, proposals exist to select an optimal model class among a set of possible
30 model classes that gives the best trade-off between data fitting and model-class complexity in order to
31 solve diagnosis and prognosis tasks [9, 15–17]. Some approaches link to Ockham’s razor [17, 18], also
32 called principle of parsimony, which asserts that simpler models that are compatible with measurements
33 are preferred over complicated ones. However, simpler models may imply over-idealization of reality and
34 consequently modeling uncertainties. Despite undeniable benefits of this principle to simplify modeling and
35 data-interpretation tasks, the question of the presence of systematic errors in the model class has not been
36 treated explicitly. Although several authors in various fields have pointed out the importance of providing
37 an adequate description of modeling uncertainties associated with the model class [4, 19–22], proposals for
38 robust alternatives to existing approaches are lacking.

39 Goulet and Smith [3] proposed an approach that is robust when knowledge of the joint PDF of modeling
40 and measurement errors is incomplete. This approach, named error-domain model falsification (EDMF),
41 combines PDFs of each source of modeling and measurement error and determines conservative probabilistic
42 thresholds that are used to falsify inadequate models. Modeling errors are estimated using engineering
43 heuristics and field observations. They have shown that this approach leads to robust parameter identification
44 in the presence of systematic errors without precise knowledge of the dependencies between modeling errors.
45 Goulet and Smith [3] also demonstrated that the assumption of independence in the common definition of
46 uncertainties in Bayesian inference may bias the posterior distribution of parameter values in the presence
47 of systematic errors. This last observation has also been noted by Simoen et al. [23]. Although Goulet
48 and Smith [3] have observed that EDMF can identify when initial assumptions related to the model class
49 are erroneous by falsifying all model instances, taking advantage of this characteristic for exploring possible
50 model classes of complex structures has not been studied.

51 Choi and Beven [24] have also observed that model falsification could serve to point out model deficiencies
52 in the search for a better model class. This observation resulted in the proposal of the generalized likelihood
53 uncertainty estimation (GLUE) framework [25] in the field of environmental modeling which is also affected
54 by large modeling uncertainties. Other examples of model-falsification procedures can be found in this field.
55 Beck [26] presented a framework for analysis of uncertainty and model selection based on recursive search and
56 model discrimination. An approach, called Monte Carlo filtering, is used for discarding sets of inadequate
57 model instances. Also, in the field of geology, Cherpeau et al. [27] proposed a fault-scenario falsification
58 approach using a misfit threshold. However in such examples, systematic errors were not included explicitly.

59 In the field of civil engineering, structural identification processes are often based on residual minimization
60 approaches [28–31], which may lead to biased results in the presence of unexpected systematic modeling
61 errors. Moon and Aktan [32] proposed a structural identification framework composed of six steps for
62 diagnosis and prognosis of complex structures. The process starts with the observation and conceptualization
63 (step 1) of the structure from which an a-priori model is developed in order to design in-situ experiments.
64 The data collected is then processed and used to identify the system for subsequent prediction by simulation
65 (step 6). In spite of the original intention by Moon and Aktan [32] for step 6 to iterate back to step
66 1, this methodology does not fully reflect the iterative aspect of data interpretation. Practice has shown
67 that, prior to interpreting measurements, engineers may not fully understand all possible model classes of
68 structural behavior. For complex structures, a non-linear backtracking procedure is often required because
69 the diagnosis task is an exploratory process involving several iterations [33] of observation and measurements,
70 data interpretation, modeling and performance predictions.

71 This paper presents a new structural identification framework based on an iterative falsification process
72 and knowledge-based reasoning. This framework is illustrated for the structural identification of a complex
73 bridge structure where several uncertainties related to the structural behavior prevents its unidirectional

74 identification. It is demonstrated that the iterative structural identification framework is able to explore
75 compatibility of several model classes of the structure by falsifying inadequate model classes. Thus, this
76 approach is able to make diagnosis and prognosis of the structural conditions using engineering heuristics
77 and on-site measurements, and is robust to modeling systematic uncertainties.

78 Section 2 describes the iterative structural identification framework along with the tasks to be performed.
79 Section 3 presents the steps of the framework applied to a full-scale bridge and a discussion of the resulting
80 diagnosis and of the possibility of making prognosis.

81 **2. Iterative structural identification framework**

82 Structural behavior diagnosis is an ill-defined inverse engineering task that is carried out in open-world
83 conditions and thus, under much uncertainty. For these reasons, such tasks usually lead to multiple explana-
84 tions for the structural health management of existing structures. The number of possible explanations may
85 be reduced by acquiring knowledge of the structural behavior. The experience and judgment of the engineer
86 as well as other forms of heuristic knowledge are thus of utmost importance. In the field of knowledge-based
87 reasoning, knowledge is acquired by new information obtained using data-interpretation tools [34]. Through
88 these tools, the engineer may test his knowledge and his hypotheses against observations.

89 Diagnosis tasks are usually solved through a process of hypothesis generation and testing. Hypotheses are
90 generated at an early stage from a basic knowledge acquired from limited information. While an early-stage
91 hypothesis may be revised or discarded if subsequent data fail to confirm it, it is likely that at least some
92 hypotheses are correct. Hypotheses are used to organize engineering knowledge and they help to reduce the
93 size of diagnosis task search space. Because it would not be possible to guide an efficient diagnosis task
94 without some hypothetical purpose, hypotheses serve to transform an open-world ill-defined task into a set
95 of well-defined deductive tasks. This process is done iteratively while gradually acquiring knowledge from
96 new observations and from rejected hypotheses.

97 In this context, the structural identification framework is governed by the principle of falsification, which
98 has been well known by scientists for centuries. However, this principle has only been popularized in the
99 1930's by Popper [35]. His philosophy stipulates that hypotheses cannot be fully validated by observations
100 and rather can only be falsified by observations. Several authors, such as Tarantola [36], Beven [37] and
101 Beck [26], underlined the advantages of this philosophy since it avoids biasing observations by hypotheses.

102 For structural identification, hypotheses are usually represented by models and observations by behavior
103 measurements. In addition, basic knowledge is composed of experience, such as information acquired by
104 structural drawings and other inspection reports that may have been established during the service life of
105 the structure, and this serves to develop early-stage hypotheses. Combining structural mechanics theory
106 with such basic knowledge is not usually sufficient for complete definition of the model class in order to

107 describe structural behavior. Thus, it is often necessary to return to previous steps in order to iteratively
 108 converge upon a correct diagnosis using several model classes.

109 In Figure 1, an iterative identification process is illustrated where the engineer is in the center of the
 110 process. Six tasks are necessary for supporting engineers; modeling, in-situ inspection, monitoring, model
 111 falsification, diagnostics and prognosis. The engineer starts anywhere and at any stage, and he might go
 112 back to previous steps. Tasks are carried out iteratively and the direction taken for the next step is based
 113 on engineering decisions based on either the information available at the current step or his knowledge.
 Data-interpretation tools are available to help engineers solve each task.

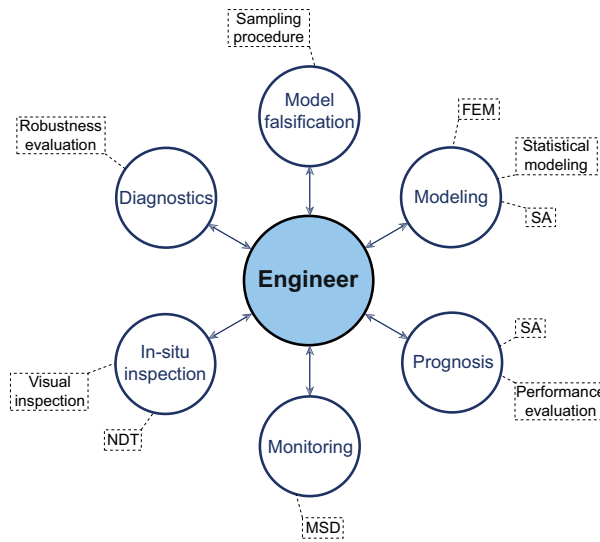


Figure 1: Iterative structural identification framework showing tasks in circles and data-interpretation tools in rectangles. Finite-element model (FEM), sensitivity analysis (SA), measurement-system design (MSD) and nondestructive testing (NDT).

114
 115 The operating principles of this framework are:

- 116 • The process is guided by the engineer who performs tasks and decides the next task to perform based
 117 on his knowledge and the information acquired in the current and previous tasks. It is likely that he
 118 would have to perform a task several times.
- 119 • Based on the principle of parsimony (Ockham’s razor), simpler model classes are preferred over more
 120 complicated classes.
- 121 • Model falsification may lead to the conclusion that modeling assumptions are not compatible with
 122 observed behavior. Especially after decades of service life, structures may behave in a complex manner
 123 because of degradation of elements. In such situations, it is important to explore a range of model

124 classes that might explain observed behavior. This exploratory approach allows the rejection of an
125 entire class of models. It is thus possible to explore the compatibility of several model classes with
126 observations. In situations where several model classes are compatible with observations, the engineer
127 may compare the performance of each model class and decide to use one or more model classes to
128 support decision making.

- 129 • Following iteration, diagnostics and prognosis are typical terminal tasks. Thus, after these tasks,
130 robustness of the results and future performance of the structure are evaluated.

131 *2.1. Modeling task*

132 The modeling task consists of building a physics-based model that describes the structural behavior and a
133 statistical model of the errors associated with the physics-based model. For the physics-based model, finite-
134 element (FE) models are most suitable for representing the behavior of complex structures. In addition, such
135 models are usually associated with uncertainties caused by unknown physical properties, simplifications and
136 omissions. Among the sources of modeling uncertainties, some may be parametrized and then identified by
137 comparing them with measurements.

138 Other sources of uncertainty may be avoided by including them explicitly in the FE model; for example,
139 components such as reinforcement bars in concrete decks, barriers, diaphragms, etc. Some sources however
140 cannot be included in the FE model either due to the time spent modeling them or due to the computational
141 demand in the FE analysis. These uncertainties may be either of random or of systematic nature. If not
142 included in the FE model, these sources of uncertainty lead to model-prediction errors that should be taken
143 into account when comparing predicted and measured responses. For this reason, errors associated with
144 the simplifications of the physics-based model are estimated for each measurement location using statistical
145 models. Special care is taken when modeling systematic uncertainties since they are usually not centered on
146 zero and are non-Gaussian [38]. Since the statistical model of modeling errors is related to the physics-based
147 model, both models define the model class.

148 Parametrized variables are usually uncertain material and geometrical properties as well as stiffness of
149 boundary conditions and connections. Among these variables, some have more influence than others on
150 the structural response. Sensitivity analysis (SA) tools may be used to distinguish the importance of these
151 variables in order to select those having the most importance to be identified [39, 40]. The number of
152 parameters to be identified is limited by the computational demand required in following tasks. However,
153 several full-scale examples of civil structures have shown that the number of parameters is usually less than
154 ten [41–43].

155 *2.2. In-situ inspection task*

156 In-situ inspection comprises visual inspection and other nondestructive testing (NDT) techniques. This
157 task includes comparing basic knowledge of the real structure with results of inspection and thus, collecting
158 information on site that would not be on structural drawings and previous inspection reports. Deterioration
159 may be detected and initial knowledge of physical properties may be revised. The engineer may then modify
160 the model class based on this information. Also, NDT techniques may provide information on material
161 properties that refine the estimation of initial model-parameter ranges and thus, help to refine the results.

162 *2.3. Monitoring task*

163 Measuring the response, either static or dynamic, at judicious locations allows the engineer to test
164 hypotheses related to the structural behavior. Measurements are able to falsify incorrect model classes
165 in order to uncover erroneous assumptions made by the engineer. They can also reduce the uncertainty
166 associated with diagnostics and prognosis tasks [43].

167 As shown by Goulet and Smith [44], more measurements does not mean higher performance of structural
168 identification. Indeed, they demonstrated that over-instrumentation appears when the new information
169 provided by additional measurements is exceeded by the amount of uncertainty provided by the additional
170 measurements. In addition, Pasquier et al. [45] argued that the higher the number of measurements used for
171 structural identification, the greater the probability of making a diagnostic error in the case of misevaluation
172 of modeling uncertainties.

173 Measurement-system-design (MSD) strategies such as [44, 46] may be used to guide the choice of mea-
174 surement locations. However, redundancy in the monitored locations is required in order to prevent the loss
175 of erroneous measurements. In addition, when performing static load tests, it is preferable to take measure-
176 ments for several load configurations in order to increase information related to the structural behavior.

177 This task also involves the choice of a subset of measurements to be compared with model predictions.
178 Subsets of measurements are usually used in a first step to limit computational demand for preliminary
179 comparison. As knowledge is acquired, the size of measurement sets may increase.

180 *2.4. Model falsification task: error-domain model falsification*

181 Proposed by Goulet and Smith [3], the error-domain model falsification approach aims to obtain possible
182 values for $\boldsymbol{\theta} = [\theta_1, \dots, \theta_{n_\theta}]^\top$, describing a vector of n_θ parameter values of a physics-based model using
183 information provided by measurements. Model parameters describe material, physical and geometrical
184 properties of a structure. Estimates for $i = 1, \dots, n_y$ characteristic responses Y_i of a structure can be
185 provided by models as well as by behavior measurements. Let $g_\kappa(x_i, \boldsymbol{\theta}_\kappa)$ denote model predictions from a
186 model class \mathcal{G}_κ and take as input the locations of the predicted degrees of freedom x_i and a set of random
187 variables Θ_κ describing parameter values $\boldsymbol{\theta}_\kappa$, \hat{y}_i denotes observations, and $\{U_{i,g_\kappa}, U_{i,\hat{y}}\}$ respectively denotes

188 random variables describing model-prediction and measurement errors for the i^{th} structural characteristic
 189 response. The relationship between a characteristic response and a model prediction is given by

$$190 \quad Y_i = g_\kappa(x_i, \Theta_\kappa) + U_{i,g_\kappa}, \quad \forall i = 1, 2, \dots, n_y \quad (1)$$

191 and between a characteristic response and a measurement is

$$192 \quad Y_i = \hat{y}_i + U_{i,\hat{y}}, \quad \forall i = 1, 2, \dots, n_y \quad (2)$$

193 The joint PDF $f_{\mathbf{U}_{\hat{y}}}(\mathbf{u}_{\hat{y}})$ describing the measurement error is in common cases estimated from repeated cal-
 194 ibration experiments performed in controlled conditions. In the case of civil structures, such estimation is
 195 usually not possible for the joint PDF of model-prediction errors, $f_{\mathbf{U}_{g_\kappa}}(\mathbf{u}_{g_\kappa})$; instead, $f_{\mathbf{U}_{g_\kappa}}(\mathbf{u}_{g_\kappa})$ is commonly
 196 estimated based on heuristics and engineering experience, including systematic errors. Examples of sources
 197 of modeling uncertainty are idealized support and connection conditions, temperature effects, load amplitude
 198 and load position, Bernoulli-beam hypothesis, geometric variability of the structure, constitutive law of ma-
 199 terials, etc. For FE models, examples are also mesh refinement and interpolation, element-type choices, the
 200 presence of singularities, etc. Since modeling uncertainty associated with complex civil structures commonly
 201 has a larger variance than measurement uncertainty, the joint PDF describing the combination of model-
 202 ing and measurement uncertainties, $f_{\mathbf{U}_c}(\mathbf{u}_c) \sim \mathbf{U}_{\hat{y}} - \mathbf{U}_{g_\kappa}$ is also dominated by heuristics and engineering
 203 experience.

204 Error-domain model falsification performs structural identification by generating an initial set of n_Ω
 205 model instances $\Omega_\kappa = \{\Theta_{\kappa,m}, m = 1, 2, \dots, n_\Omega\}$ of a model class \mathcal{G}_κ and then falsifies instances that are not
 206 compatible with observations given measurement uncertainties and modeling uncertainties associated with
 207 the model class \mathcal{G}_κ . The candidate model set Ω_κ^* consists of the initial model set minus the falsified models
 208 so that

$$209 \quad \Omega_\kappa^* = \{\theta_\kappa \in \Omega_\kappa : u_{i,\text{low}} \leq g(x_i, \theta_\kappa) - \hat{y}_i \leq u_{i,\text{high}}, \forall i\} \quad (3)$$

210 where $u_{i,\text{low}}$ and $u_{i,\text{high}}$ are threshold bounds defining the shortest intervals including a probability ϕ_d^{1/n_y} for
 211 the marginal PDFs of $f_{\mathbf{U}_c}(\mathbf{u}_c)$, where $\phi_d \in [0, 1]$ is the target identification reliability usually set at 0.95.
 212 In addition, the number of model instances in the candidate-model set is n_{Ω^*} and each instance is equally
 213 likely to be the correct representation of the structure.

214 All model instances that have been falsified are assigned a probability of 0 so that

$$215 \quad \Pr(\Theta_\kappa = \theta_\kappa \notin \Omega_\kappa^*) = 0 \quad (4)$$

216 and all model instances belonging to the candidate-model set are assigned a constant probability

$$217 \quad \Pr(\Theta_\kappa = \theta_\kappa \in \Omega_\kappa^*) = \frac{1}{\int_{\theta_\kappa \in \Omega_\kappa^*} d\theta_\kappa} \quad (5)$$

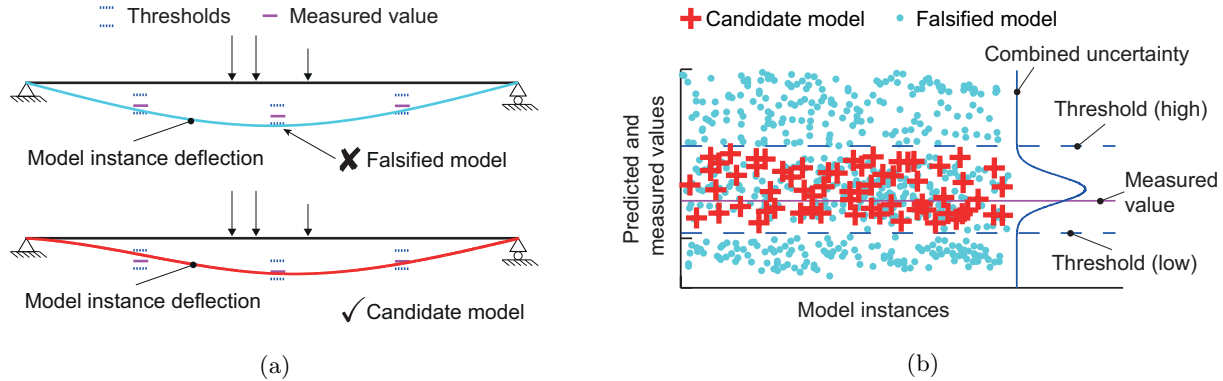


Figure 2: Model falsification example for a simple beam. (a) Model-instance falsification and acceptance using three measurements. (b) Sensor plot describing the falsification of a set of model instances for a single measurement location. Falsified model predictions that lay within the threshold bounds are predictions of model instances that are falsified at other measurement locations.

218 Figure 2a presents examples of falsification and acceptance of a model instance for a simple beam based
 219 on three measurement locations. A model instance which predictions do not lay within the threshold bounds
 220 for the three locations is falsified. A model instance with a different combination of parameter values which
 221 predictions lay within the thresholds for every location is a candidate model. Figure 2b shows a sensor
 222 plot which compares a single measured value with the predictions of the initial model set and the threshold
 223 bounds. Candidate-model predictions are within the thresholds. Falsified model predictions that lay within
 224 the threshold bounds are predictions of model instances that are falsified at other measurement locations.

225 In some cases, it is possible that EDMF leads to $\forall \theta_{\kappa} : \Pr(\Theta_{\kappa} = \theta_{\kappa}) = 0$ which results in the complete
 226 falsification of the initial population of model instances, $\Omega_{\kappa}^* = \emptyset$. This means that there is a likely error
 227 in assumptions that led to model-class building and thus, the model class \mathcal{G}_{κ} is falsified. Such diagnosis
 228 guides the engineer to search for erroneous assumptions and to explore alternative model classes that may
 229 be compatible with the set of measurements.

230 In practice, a sensitivity analysis is carried out during the modeling task (see Section 2.1) for determining
 231 the relative importance of each uncertainty source. The uncertainty of the model response at the measured
 232 locations due to the parametrized sources are evaluated through Monte Carlo sampling and the FE model.
 233 Parametrized sources that have the major importance are included in the primary parameter vector θ_{κ} and
 234 are used to generate the initial model set Ω_{κ} . Parametrized sources with minor importance are included
 235 in the secondary parameter vector $\gamma_{\kappa} = [\gamma_1, \gamma_2, \dots, \gamma_{n_{\gamma}}]^T$. These secondary parameters induce modeling
 236 uncertainties $\mathbf{V}_{g_{\kappa}}$ that should be taken into account when comparing model predictions with measurements.
 237 The secondary parameter uncertainties are given by

$$238 \quad \mathbf{V}_{g_{\kappa}} = g(\mathbf{x}, \bar{\theta}_{\kappa}, \mathbf{\Gamma}_{\kappa}) - g(\mathbf{x}, \bar{\theta}_{\kappa}, \bar{\gamma}_{\kappa}) \quad (6)$$

239 where secondary parameters γ_κ are described by random variables Γ_κ , and $\bar{\theta}_\kappa$ and $\bar{\gamma}_\kappa$ are mean values of
 240 Θ_κ and Γ_κ .

241 Other sources of uncertainties, \mathbf{W}_{g_κ} , are estimated based on heuristics and engineering experience as
 242 presented in Section 2.1. \mathbf{V}_{g_κ} is added to the other modeling uncertainties \mathbf{W}_{g_κ} , such that the combined
 243 uncertainties

$$244 \quad \mathbf{U}_c = \mathbf{U}_{\hat{y}} - \mathbf{U}_{g_\kappa} = \mathbf{U}_{\hat{y}} - (\mathbf{V}_{g_\kappa} + \mathbf{W}_{g_\kappa}) \quad (7)$$

245 In this way, systematic and zero-mean random modeling uncertainties are included in the model-falsification
 246 process. Note that usually, the simpler the FE model, the greater the variance of the modeling uncertainty
 247 \mathbf{U}_{g_κ} , which cannot be reduced using model falsification. Conversely, the random uncertainty associated with
 248 primary parameters θ is reduced by the information provided by measurements.

249 Several sampling techniques are available in order to generate the initial model set Ω_κ . Depending on the
 250 number of parameters n_θ and precision of the identified parameter values, either uniform sampling or Latin
 251 hypercube sampling (LHS) is used. If necessary, Markov Chain Monte Carlo sampling [18] may be used
 252 in situations where LHS leads to excessive computation times. Structural identification of existing bridges
 253 commonly necessitates less than ten parameters. Whatever sampling method is used, the initial distribution
 254 of the parameter values is usually uniform with bounds determined based on engineering judgment and
 255 depending on the nature of the physical parameter.

256 *2.5. Diagnostics task*

257 The diagnostics is the task that makes sense of the identification results of physical properties of the
 258 structure and leads to conclusions about the structural conditions. When the model class is compatible with
 259 the set of measurements, a candidate model set is identified, $\Omega_\kappa^* \neq \emptyset$, and candidate parameter values are
 260 determined. This solution may be used to confirm assumptions about the structural behavior that were
 261 made during the modeling task and thus increase the knowledge of the structural behavior.

262 Robustness-evaluation techniques may be used to determine the diagnostic sensitivity to conditions such
 263 as miscalculation of uncertainties and changes in correlations between measurements at different measurement
 264 locations. These tools provide help in minimizing the false positive and false negative diagnostics either at
 265 the model-class or the model-instance level.

266 For example, when performing structural identification with a high number of sensors and several load
 267 cases, some measurements may have faulty behavior during load tests. These measurements may not be
 268 detected using engineering common sense and outlier detection procedures. However, these measurements
 269 may either bias the diagnostics or wrongly falsify a correct model class. A study of the sensitivity to
 270 erroneous measurements is thus conducted in order to evaluate diagnosis robustness. For this purpose, it
 271 is proposed to carry out model falsification iteratively by removing individually each measurement under
 272 any load case. Thus, $n_y - 1$ measurements are compared with model predictions for each iteration. In a

273 second step, each measurement is removed one by one for every load case since it is likely that an erroneous
 274 measurement remains erroneous during other load cases. During the two processes, the number of candidate
 275 models obtained for each iteration is stored and the sensitivity to erroneous measurements can be evaluated
 276 through the variation in the number of candidate models.

277 2.6. Prognosis task

278 This task involves using identification results for predicting quantities under conditions other than those
 279 prevailing during monitoring, for example, model extrapolation for other load configurations [14]. An ex-
 280 ample in the field of civil engineering is prediction of remaining fatigue life of bridge critical details under
 281 traffic loads [43]. The results of prognosis tasks lead to important knowledge necessary for decision making
 282 involving retrofit, repair and replacement of existing structures. In this framework, predictions are performed
 283 based on the candidate models obtained using EDMF. The prediction of a quantity q_j at n_q locations of a
 284 structure is given by

$$285 \quad Q_j = g(x_j, \Theta_\kappa^*) + U_{j,g_\kappa}, \quad \forall j = 1, \dots, n_q \quad (8)$$

286 in agreement with Eq. (1), where Θ_κ^* is described by the PDF

$$287 \quad f_{\Theta_\kappa^*}(\theta_\kappa) = \begin{cases} \frac{1}{\int_{\Omega_\kappa^*} d\theta_\kappa}, & \text{if } \theta_\kappa \in \Omega_\kappa^* \\ 0, & \text{otherwise} \end{cases} \quad (9)$$

288 that is based on Eq. (4) and (5). Thus, Q_j is a random variable describing the distribution of the predicted
 289 quantity q_j that is obtained by the combination of the predictions of random candidate-model instances
 290 and the distribution of modeling uncertainties associated with model class \mathcal{G}_κ at the j^{th} prediction location,
 291 U_{j,g_κ} . The lower and the higher threshold bounds of Q_j are then determined based on the target prediction
 292 reliability $\phi_p \in [0, 1]$ usually set at 0.95. They define the shortest intervals including a probability ϕ_p^{1/n_q}
 293 for each PDF Q_j . Consecutively, since the identification reliability is ϕ_d , the probability of having the
 294 true prediction value included between prediction thresholds for each location is at least $\phi_d \cdot \phi_p$, given the
 295 estimated PDF of uncertainty.

296 Prognosis performance evaluation may be carried out in order to determine whether or not the uncertainty
 297 associated with the predicted quantity is acceptable for making good decisions regarding the management of
 298 the structure. In situations where the prediction is too uncertain, sensitivity analysis may be used to identify
 299 the main uncertainty sources and guide the engineer in the next iteration of the framework. Examples of
 300 next steps are monitoring at locations that are related to high uncertainty sources and intervention in order
 301 to either repair or replace bridge components that contribute to uncertainty.

302 2.7. Framework summary and example

303 The proposed framework supports structural identification based on an iterative falsification process and
 304 reasoning with engineering knowledge. This approach is suitable for ill-defined tasks such as structural

305 identification where information is obtained gradually. The engineer is at the core of the process and makes
 306 decisions regarding next steps among the six tasks in order to increase knowledge of structural behavior.

307 An example of this process is presented in Figure 3 where arrows describe engineering decisions. It starts
 308 with an in-situ inspection, continues with the model-class modeling based on structural drawings, then
 309 monitoring of judicious locations and model falsification using these measurements. In this case, the model
 310 class is falsified due to erroneous assumptions in the preliminary modeling task and thus no diagnostics is
 311 provided. The engineer decides to further inspect the structure in order to understand the cause of model-
 312 class falsification. After correction of the model class, the model falsification returns candidate models from
 313 which structural diagnosis is possible. In the last step, a prognosis can be made in the scope of structural
 314 management decision making. If the performance evaluated in the prognosis step is adequate, the process
 315 ends and the engineer makes a decision. In the case where the prognosis is too uncertain, the engineer
 316 may decide to perform additional structural monitoring, focusing on the locations that induce high behavior
 uncertainty.

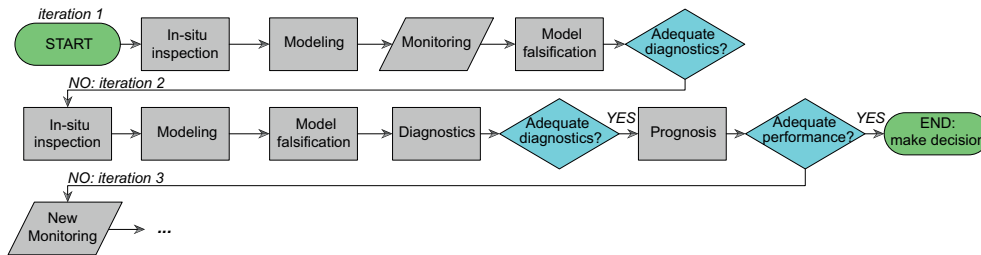


Figure 3: Iterative structural identification process example.

317

318 3. Case study: full-scale bridge in Wayne, New Jersey

319 This thirty-year-old bridge carries US202/NJ23 through Wayne, in New Jersey (USA). The bridge carries
 320 eight traffic lanes over four simply-supported spans. The focus is on the second southbound span four lanes
 321 that are displayed in Figure 4a. This bridge span has eight steel girders acting in a composite manner
 322 with a concrete deck (see Figure 4b). The span geometry is skewed and slightly curved in elevation. The
 323 straight-side girders are supported by eight fixed bearing devices and the skewed-side girders are supported
 324 by expansion bearing devices. A static load test is carried out using several truck load-case configurations
 325 and measuring, for each configuration, twelve vertical displacements (see Figure 5).

326 Displacement sensors were positioned in a grid manner on the bottom flanges of girders 1, 3, 6 and 8 at
 327 the quarter, half and three quarter spans. Load configurations of LC-1 to LC-3 consisted of three full trucks
 328 positioned on three lanes at the quarter, half and three quarter spans. The fourth lane was open to traffic

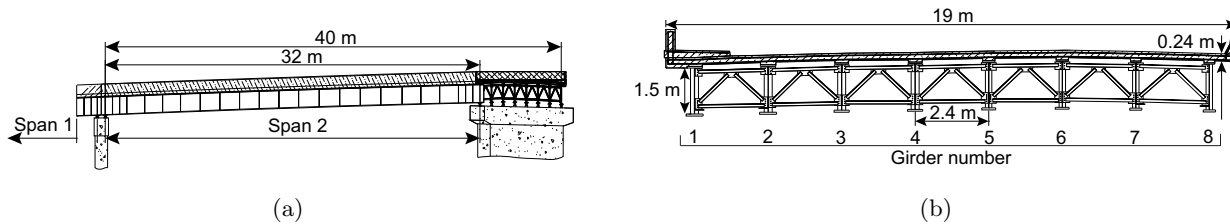


Figure 4: (a) Bridge elevation view; (b) bridge cross-section view (Adapted from [38]).

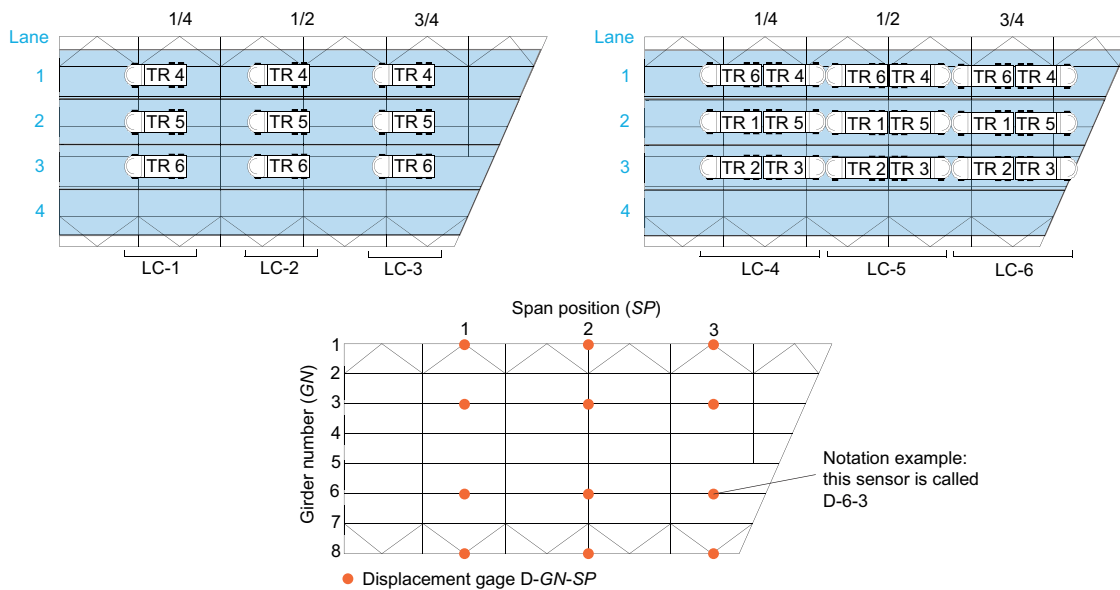


Figure 5: Configurations of static-load tests and displacement gages: six load cases (LC) using six trucks (TR) and twelve displacement gages named as D-GN-SP.

329 during the static load test. For LC-4 to LC-6, the position was similar and the configurations involve six full
330 trucks weighing around double of the load in LC-1 to LC-3.

331 Structural identification is carried out using four load cases (LC-1, 2, 3 and 5) and the twelve vertical
332 displacements as shown in Figure 5. Load cases LC-4 and LC-6 are kept for the verification of the identifi-
333 cation results. This bridge is a typical example of an aging structure that needs better management. The
334 objective of structural identification is to make a diagnosis for structural health management and discuss
335 the possibility of making a prognosis. The iterative structural identification framework presented in Section
336 2 is used to perform this task.

337 3.1. Identification framework iteration 1

338 The structural identification framework first iteration starts with the monitoring phase where the full
339 data set is acquired. The next step of the framework is modeling using the basic knowledge acquired from
340 structural drawings and engineering experience. The engineer decides to build a FE model. When modeling
341 such a complex structure, several assumptions are made resulting in modeling uncertainties. Some sources of
342 modeling error have a random nature while other sources are systematic; they are caused by aspects such as
343 inappropriate model forms and simplified boundary conditions. When the FE model does not account for a
344 source of uncertainty, the modeling uncertainty induced has to be taken into account when comparing model
345 predictions with measurements. Thus, the more aspects included in the FE model, the less uncertainties
346 to be taken into account for the model falsification task and the better performance obtained for structural
347 identification.

348 For the performance of structural identification, a detailed 3D FE model whose model predictions are
349 described by $g_1(\mathbf{x}, \cdot)$ is built. The rows of matrix $\mathbf{x} = x_{kl}$ represents the prediction locations $k \in \{1, 2, \dots, 12\}$
350 related to the measured locations and the columns, the load cases $l \in \{1, 2, \dots, 6\}$ under which the predictions
351 are calculated. Each element in x_{kl} refers to a measurement location i in Section 2.4 and the number of
352 elements is thus equal to the number of measurements n_y . This model includes the concrete deck with
353 reinforcement bars, concrete barriers and the sidewalk, wind-braces, diaphragms and stiffeners as shown in
354 Figure 6. Also, special care is taken to include the bridge curvature, distributed truck-wheel loads instead
355 of ideal point loads and the support eccentricity to the cross-section center (see Figure 7 and 8). For the
356 connection of the girder bottom flange and the bearing pin, rigid links are used such that the rotation of
357 the girder is rigidly transmitted to the pin. In order to allow the longitudinal displacement of the expansion
358 bearing, a pinned rigid link connects the central pin to the bottom bearing. By releasing only the rotational
359 degree of freedom of the bottom pin, the displacement of the central pin is possible. Since friction may
360 exist in the pin, rotational springs are modeled with unknown rotational stiffness parameter values γ_{rot} .
361 Parametrized uncertainty sources such as material Young's moduli (γ_{conc} and γ_{steel}), the Poisson's ratio of
362 concrete ($\gamma_{\Delta\nu}$), the thickness of the concrete deck ($\gamma_{\Delta T}$) and steel plates ($\gamma_{\Delta t}$) and truck loads ($\gamma_{\Delta w}$) are

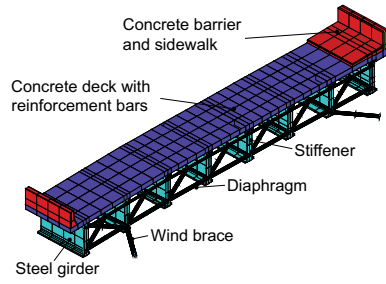


Figure 6: Bridge finite-element model.

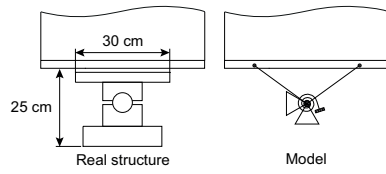


Figure 7: Real and modeled fixed bearing device.

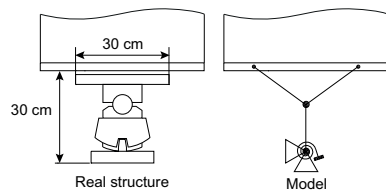

















Figure 8: Real and modeled expansion bearing device.

363 also parametrized. These sources and their statistical models are displayed in Table 1 from #1 to #7. Their
 364 PDFs describe the uncertainty associated with their parameter value γ that is estimated using engineering
 365 heuristics and field observations. Their effects on the structural response is then quantified through Monte
 366 Carlo simulations using the FE model and Eq. (6).

Table 1: Sources, probability density functions and relative importances of modeling and measurement uncertainties for identification framework iteration 1. PDFs of sources #1 to #7 are related to their parameter values. PDFs of sources #8 to #15 are associated with characteristic responses. The relative importance values are averaged over all measurement locations.

Uncertainty source	PDF	Unit	Mean/Min	SD/Max	Relative importance
1. Rotational stiffness of bearings	log-uniform	log(Nmm/rad)	6	12	47 % 
2. Young's modulus of concrete	Gaussian	GPa	21.5	4.5	16 % 
3. Young's modulus of steel	Gaussian	GPa	200	5	3.4 % 
4. $\Delta\nu$ Poisson's ratio of concrete	Gaussian ^a	-	0	0.025	2.4 % 
5. ΔT concrete deck thickness	Gaussian	%	0	2.5	1.3 % 
6. Δt steel plate thickness	Gaussian	%	0	1	1.9 % 
7. Δw truck load per wheel	Gaussian	N	0	225	0.7 % 
8. Simplifications and FEM	uniform	%	-8	1	4.3 % 
9. Mesh refinement	uniform	%	-1	0	0.9 % 
10. Truck position	Gaussian	%	-1	0.8	2.7 % 
11. Sensor resolution	Gaussian	mm	0	0.13	12 % 
12. Cable losses	Gaussian	%	0	0.4	1.5 % 
13. Repeatability	Gaussian	%	0	0.5	2.0 % 
14. Traffic noise	Gaussian	mm	0	0.02 - 0.1 ^b	2.7 % 
15. Additional uncertainties	Gaussian	%	-1	1	1.2 % 

^aGaussian distribution that is truncated at 0.03 and 0.33.

^bMinimum and maximum standard deviation over all measured values.

367 For the rotational stiffness of bearings, the range of values is evaluated based on the relation between the
 368 stiffness value and the displacement responses that are represented in Figure 9. This figure shows that for
 369 values lower than 10^6 Nmm/rad and values higher than 10^{12} Nmm/rad, the response is not sensitive to the
 370 stiffness value. For such ranges of values, the bearing acts either as a pinned or as a fixed support. Thus,
 371 the initial significant parameter range is between 10^6 and 10^{12} where the parameter value influences the
 372 response.

373 The other sources of uncertainty that cannot be included in the FE model are estimated using engineering
 374 judgment with respect to model predictions generated with the mean value of the parameters #1 to #7.

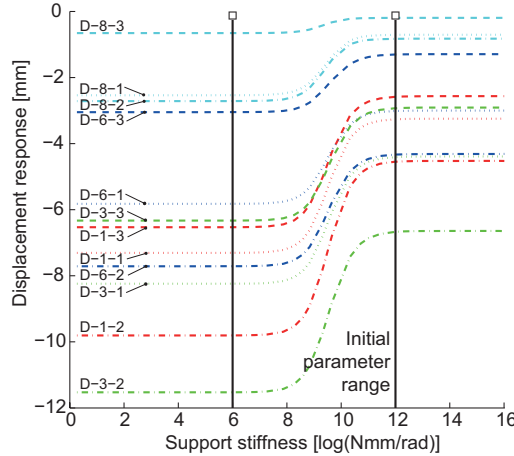


Figure 9: Relation between support rotational stiffness values and displacement responses.

375 These sources listed in Table 1 from #8 to #10 are model simplifications and FEM idealization (\mathbf{W}_{simp}), mesh
 376 refinement (\mathbf{W}_{mesh}) and truck position (\mathbf{W}_{tp}). For source #8, simplifying assumptions are the non-inclusion
 377 of concrete-deck cracks, partially connected barrier, barrier joints that reduce the predicted displacement. In
 378 addition, FE models are usually stiffer than reality. Thus, these aspects lead to overestimate displacement
 379 predictions. The lower bound -8% was determined based on this reasoning and engineering judgment. The
 380 non-inclusion of the fence, which increases predicted displacements, explains the value of $+1\%$ of the upper
 381 bound of source #8. An extensive description of sources and forms of uncertainties is available in [38].

382 In order to compare model predictions and measurements, measurement uncertainties are also estimated
 383 (#11 to #15). These sources are sensor resolution (\mathbf{U}_{res}), cable losses (\mathbf{U}_{loss}), measurement repeatability
 384 (\mathbf{U}_{rep}) and traffic noise (\mathbf{U}_{traf}) during static load tests. Additional uncertainties (\mathbf{U}_{add}) are a conservative
 385 estimation for all other phenomena that individually have a negligible influence.

386 Table 1 also presents the relative importance of each uncertainty source on the structural response. This
 387 relative importance is averaged over all measurement locations under all load configurations. This shows
 388 that the rotational stiffness of bearings is the main source of uncertainty with 47% of influence. The second
 389 most important source is the Young's modulus of concrete with 16% relative importance. Due to their high
 390 influence on the structural response, these two parameters are selected to generate the initial model set. The
 391 other parametrized uncertainties have too low of an influence to be identifiable. However, they are included
 392 with the remaining uncertainties in $f_{\mathbf{U}_c}(\mathbf{u}_c)$ as described in Eq. (7) for the calculation of threshold bounds
 393 during the falsification process. Note also the high influence of the sensor resolution with 12% relative
 394 importance.

395 The first model class \mathcal{G}_1 is thus composed of $g_1(x_{kl}, \boldsymbol{\theta}_1)$ with $\boldsymbol{\theta}_1 = [\theta_{\text{rot}}, \theta_{\text{conc}}]^\top$ being the rotational
 396 stiffness and the Young's modulus of concrete, and the combination of modeling uncertainties #3 to #10,

397 \mathbf{U}_{g_1} displayed in Table 1 and calculated using Eq. (10).

$$398 \quad \mathbf{U}_{g_1} = \mathbf{V}_{\text{steel}} + \mathbf{V}_{\Delta\nu} + \mathbf{V}_{\Delta T} + \mathbf{V}_{\Delta t} + \mathbf{V}_{\Delta w} + \mathbf{W}_{\text{simp}} + \mathbf{W}_{\text{mesh}} + \mathbf{W}_{\text{tp}} \quad (10)$$

399 Measurement uncertainties are combined based on Eq. (11).

$$400 \quad \mathbf{U}_{\hat{y}} = \mathbf{U}_{\text{res}} + \mathbf{U}_{\text{loss}} + \mathbf{U}_{\text{rep}} + \mathbf{U}_{\text{traf}} + \mathbf{U}_{\text{add}} \quad (11)$$

401 The rotational stiffness value is the same for all 16 supports since there is no information at this step regarding
 402 different stiffnesses of bearing devices. The next step involves the model falsification and the initial model
 403 set is generated based on a uniform sampling for which the range given in Table 1 is divided into 11 intervals
 404 for both parameters, leading to a set $\Omega_1 = \{\Theta_1\}$ of $n_{\Omega_1} = 144$ model instances. Using $n_y = 24$ displacement
 405 measurements of load cases LC-2 and 5 (in x_{kl} , $l \in \{2, 5\}$). Only a subset of the measurement data set is
 406 used to reduce the computing demand of the initial iteration.

407 This process leads to the complete falsification of the initial model set and thus the falsification of model
 408 class \mathcal{G}_1 . As a result, no diagnostic can be provided and a likely error is present in assumptions that led to
 409 model-class building.

410 *3.2. Identification framework iteration 2*







411 Since at this stage, information is lacking regarding the source of this model-class error, the engineer
 412 decides to make in-situ visual inspection for the purpose of comparing his prior assumptions about the
 413 structure with the real structure. Thus, a second iteration of the identification framework starts. On site,
 414 a penetrating crack is observed on the pier cap under the support of girder 1 on the straight bridge side.
 415 This crack may reduce the stiffness of the pier cap and thus the assumption of infinite vertical stiffness
 416 of the support is no more valid. In addition, a severe state of corrosion deterioration is observed on the
 417 bearing devices, particularly on the exterior bearing devices, i.e. the supports of girder 1 and 8. The visual
 418 inspection also reveals that the concrete deck is orthotropic by observing a steel deck plate on the lower side
 419 of the bridge.

420 In the next step of the identification process, the engineer decides to include the components observed
 421 during in-situ inspection in a new model class \mathcal{G}_2 . The FE model is modified to incorporate the orthotropic
 422 deck and a vertical spring with unknown stiffness under the support where the pier cap crack is located.
 423 The spring stiffness is another uncertain parameter that adds to the other modeling uncertainties. A similar
 424 study of the relation parameter value to displacement response as the one of the rotational spring stiffness
 425 (see Figure 9) is undertaken. This study leads to a significantly sensitive range of values between 10^2 and
 426 10^8 N/mm.

427 In order to include the effect of the severe corrosion of the exterior bearings, two distinct parameters are
 428 used to describe either the uncertainty of the averaged stiffness of the exterior bearings (i.e. bearings under

girder 1 and 8) or the averaged stiffness of the interior bearings. Although larger stiffness values are expected on the exterior bearing than on the interior's, the range of values of both parameters remains identical as the values displayed in Table 1. Table 2 presents the sources and the relative importances of uncertainties associated with the identification of model class \mathcal{G}_2 .

Table 2: Sources and relative importances of parameter, modeling and measurement uncertainties for identification framework iteration 2. The relative importance values are averaged over all displacement measurement locations.

Uncertainty source	Relative importance
Exterior bearing rotational stiffness	14 % 
Interior bearing rotational stiffness	32 % 
Young's modulus of concrete	16 % 
Modeling uncertainties	18 % 
Measurement uncertainties	19 % 
Pier-cap stiffness	1.0 % 

Exterior and interior bearing stiffnesses and the Young's modulus of concrete have a high importance and thus are selected as identification parameters. The pier-cap stiffness uncertainty (\mathbf{V}_{pier}) has very low influence on the displacement response and thus is added to modeling uncertainties \mathbf{U}_{g_1} , which remains in this model class, for the determination of \mathbf{U}_{g_2} as described by

$$\mathbf{U}_{g_2} = \mathbf{U}_{g_1} + \mathbf{V}_{\text{pier}} \quad (12)$$

where \mathbf{U}_{g_2} is then used for the determination of $f_{\mathbf{U}_c}(\mathbf{u}_c)$.

As a result, the new model class \mathcal{G}_2 is composed of $g_2(x_{kl}, \boldsymbol{\theta}_2)$ with parameters $[\theta_{\text{rot-ext}}, \theta_{\text{rot-int}}, \theta_{\text{conc}}]^T$ to identify and the modeling uncertainties \mathbf{U}_{g_2} based on Eq. (12). For the next model-falsification step, an initial model set is generated based on a uniform sampling of the three parameters $\boldsymbol{\theta}_2$. Each parameter range is divided into 11 intervals leading to an initial set $\Omega_2 = \{\boldsymbol{\Theta}_2\}$ of $n_{\Omega_2} = 1,728$ model instances of model class \mathcal{G}_2 . Using the $n_y = 24$ displacement measurements of LC-2 and 5, no compatibility is found between the model instances and the measurements ($\Omega_2^* = \emptyset$). Model class \mathcal{G}_2 is also falsified. The diagnostics of iteration 2 is thus inadequate.

In order to locate the source of the erroneous assumptions leading the falsification of the model class, the measurements of LC-1 and 3 are also included in the set of measurements used for model falsification. Then, subsets of the measurement set are used in order to identify candidate models. By successively selecting the 12 displacements of a single load case, it is observed that only LC-2 and LC-3 are able to identify candidate models. When selected together, these load cases identify 11 candidate models.

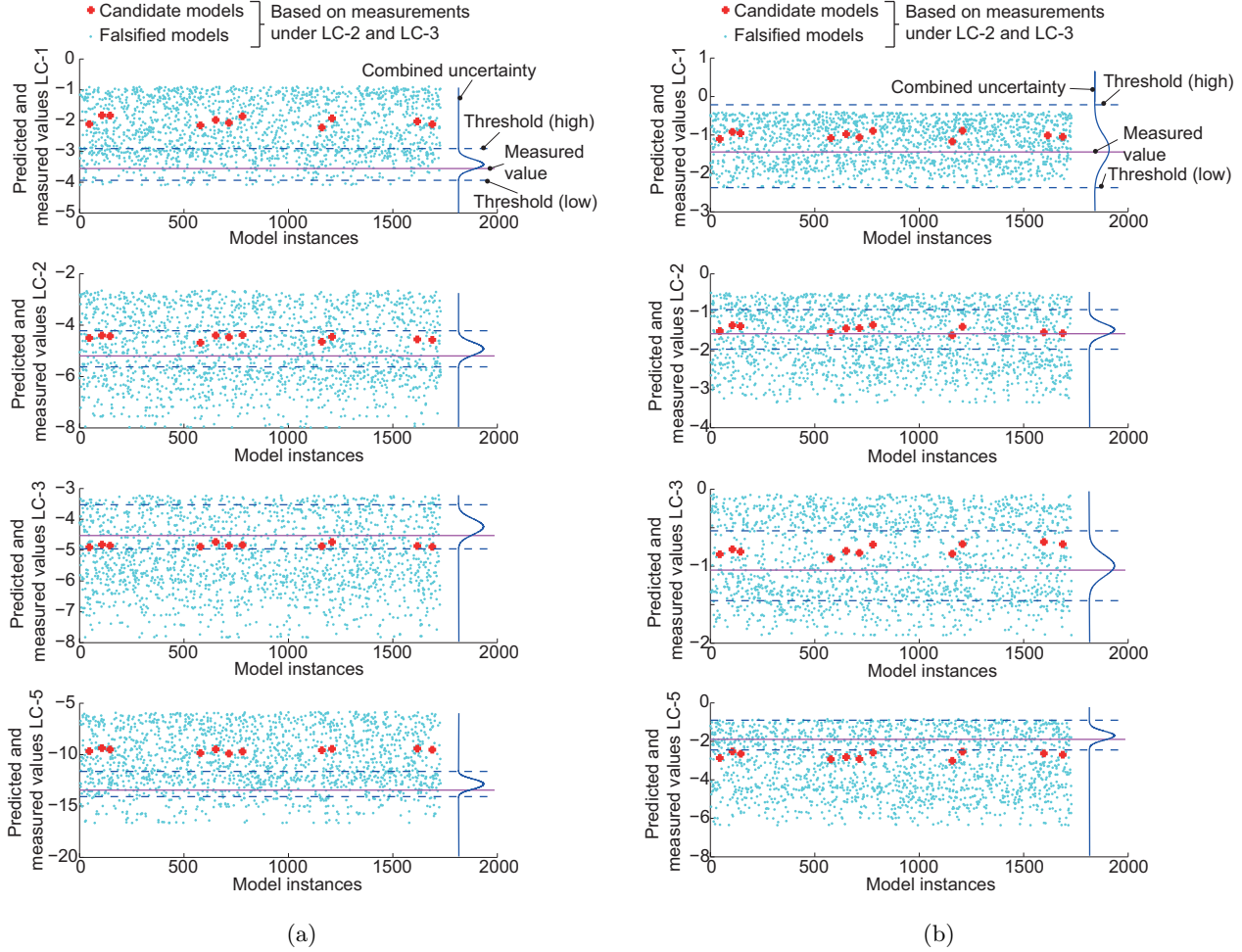


Figure 10: Comparison of model predictions and measured values for LC-1, 2, 3 and 5. (a) Sensor D-3-3 ; (b) Sensor D-8-1.

451 Figures 10a and 10b show the initial model predictions (dots) and the eleven candidate-model predictions
 452 (crosses) for sensors D-3-3 and D-8-1. In these figures, the measured values, the combined uncertainty and
 453 the threshold bounds are also represented. Under LC-2 and LC-3, the candidate-model predictions lay in
 454 the region bounded by the thresholds. Predictions that are between the threshold bounds and that are
 455 not candidate-model predictions are predictions from model instances that are falsified by the other sensor
 456 locations of LC-2 and LC-3.

457 Candidate-model predictions of LC-1 and LC-5 lay outside the region bounded by the thresholds for
 458 sensor D-3-3. These predictions reflect an over-stiff behavior of the candidate models for these locations.
 459 Note that this behavior is common to all sensors located on girders 1 and 3. In addition, for sensor D-8-1
 460 under LC-5, candidate-model predictions reflect that candidate-model instances have a softer response than
 461 that which was measured. Note also that this behavior is common to sensor D-8-2. The sensor plot of D-8-1

462 under LC-1 depicts an example of a redundant sensor, i.e. a sensor that is not able to falsify additional
 463 model instances.

464 These observations may be correlated with the in-situ measurements as a result of the stepwise increasing
 465 loading that is used during static load tests. Figure 11 presents the relation between measured displacement
 466 values for several sensors and the truck load on the bridge for configurations of trucks positioned at the
 467 quarter, half and three quarter spans. This figure involves LC-1 to LC-6 and also empty-truck load cases that
 468 are not represented in Figure 5 and not used for identification since the amplitude of measured displacement
 values is not high enough compared with the sensor resolution to be used for structural identification. This

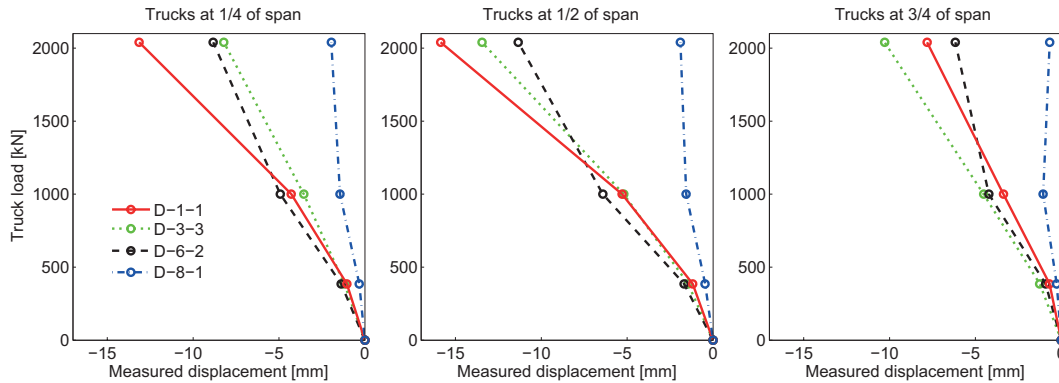


Figure 11: Non-linear relation of displacement responses and truck loads for trucks positioned at the quarter, half and three quarter of the bridge span.

469 figure depicts a non-linear relation between displacement and loading. In addition, for sensors D-1-1 and
 470 D-3-3, the behavior is softer as the loading increases and for sensors D-6-2 and D-8-1, the behavior is stiffer in
 471 the same conditions. Note that these trends are similar for the majority of measurements. Thus, observations
 472 made in Figure 10a and particularly the underestimation of the displacements made by the candidate-model
 473 instances is thus caused by the non-linear behavior observed in Figure 11 since the model class \mathcal{G}_2 assumes a
 474 linear behavior under increasing loading conditions. The same correlation can be made between the sensor
 475 plot of D-8-1 in Figure 10b and the behavior of displacement values with increasing loading, except that in
 476 this case the candidate-model predictions overestimate the displacement values due to the stiffer observed
 477 behavior.
 478

479 From the severe corrosion of the bearing devices that is observed during in-situ inspection and the high
 480 influence of the stiffness in the displacement response of the bridge, it can be deduced that non-linear
 481 behavior is caused by the bearing devices. Indeed, the non-linear concave behavior observed on girders 1
 482 and 3 may be the result of the corrosion that creates a high rotational stiffness on the support for low loading
 483 values and this blocking may be released for increasing loads due to increasing moment at support. This
 484 behavior does not appear for girders 6 and 8 that have a shorter span than girders 1 and 3 and rather, an

485 increasing load may further block the bearings due to low values of moments in these supports. Based on
 486 these observations, the engineer decides to start a third iteration.

487 3.3. Identification framework iteration 3

488 This new iteration of the identification framework starts with the modeling of non-linear spring behavior
 489 of the bearing devices. As more information is not available, it is assumed that the bearings follow a bilinear
 490 rotation-moment relation instead of the linear behavior that has been modeled up until this point. Figure 12
 491 shows a schematic description of the bilinear relationship and the unknown parameters C_1 , C_2 and φ that
 describe the behavior of the bearings. The parameters C_1 and C_2 represent the stiffnesses of the rotational

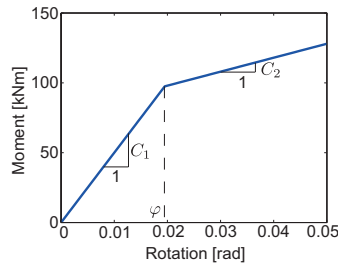


















Figure 12: Schematic bilinear model of the moment-rotation relationship of the bearing devices.

492
 493 springs and φ the rotation value for which the stiffness changes from C_1 to C_2 . Based on the behavior
 494 observed in Figure 11, the value of C_1 may be higher or lower than the value of C_2 and may be different
 495 for each bearing device. Their initial range of values is thus the same as the ranges of rotational stiffness
 496 values of model classes \mathcal{G}_1 and \mathcal{G}_2 presented in Table 1. Based on bearing rotation values obtained with the
 497 11 candidate models of the previous falsification, a conservative range of values is estimated for φ between
 498 0 and 0.03 radians. Note that a value of 0 rad implies a linear relationship with C_2 as single parameter.

499 In order to identify the bearing stiffnesses having the main influence in the bridge response and thus
 500 reduce the number of parameters θ , a sensitivity analysis is carried out by varying the stiffness value of
 501 all bearings. Table 3 presents the relative importance of the stiffness parameter for each bearing device
 502 for the linear FE model. The rotational stiffness of the bearings located on the skewed bridge side show a
 503 significantly greater importance than the bearings located on the other side. This means that the influence of
 504 a potential non-linear behavior of the straight-side bearing devices is negligible, and thus, they are modeled
 505 with linear behavior.

506 As a result, the identification parameters of the new model class \mathcal{G}_3 includes only the stiffness parameters
 507 of the skewed side and thus, the unknown parameters of the bilinear model are selected only for these bearings.
 508 This reduces the number of parameters to identify from 49 to 25 (i.e. C_1 , C_2 and φ for each bearing on
 509 the skewed side and the Young's modulus of concrete) and $\theta_3 = [\theta_{\text{rot-1s-}C_1}, \theta_{\text{rot-1s-}C_2}, \theta_{\text{rot-1s-}\varphi}, \dots, \theta_{\text{conc}}]^T$. In

Table 3: Relative importance of rotational stiffness parameter of the 16 bearings. The relative importance values are averaged over all measurement locations. For the stiffness parameters, the number refers to the girder and "s" refers to bridge skewed side.

Stiffness parameter	Relative importance
rot-1	1.1 % 
rot-2	0.8 % 
rot-3	1.3 % 
rot-4	1.0 % 
rot-5	1.8 % 
rot-6	1.5 % 
rot-7	1.2 % 
rot-8	1.7 % 
rot-1s	17 % 
rot-2s	8.4 % 
rot-3s	8.1 % 
rot-4s	8.1 % 
rot-5s	11 % 
rot-6s	14 % 
rot-7s	12 % 
rot-8s	11 % 

510 addition, the modeling uncertainties include the uncertainty associated with stiffness values of linear-behavior
 511 bearings rot-1 to rot-8:

$$512 \quad \mathbf{U}_{g_3} = \mathbf{U}_{g_2} + \sum_{r=1}^8 \mathbf{V}_{\text{rot-}r} \quad (13)$$

513 Since the number of parameters is too high to generate the initial model set using uniform sampling, Latin-
 514 hypercube sampling is employed to generate the initial model set $\Omega_3 = \{\Theta_3\}$ of $n_{\Omega_3} = 10,000$ model instances
 515 of model class \mathcal{G}_3 . However, in this model-falsification step, all model instances are falsified leading to the
 516 rejection of model class \mathcal{G}_3 . This means that the assumed bilinear behavior of the bearings is an erroneous
 517 assumption. This implies that the real behavior of the bearing is more complex than this simplified bilinear
 518 model. In addition, although the corrosion of the bearings is an important source of non-linear behavior, the
 519 geometrical complexity introduced by the skewed bridge side may also add some difficulties when identifying
 520 the true behavior of the bearings. Indeed, under some load cases, support reactions under girder 8 appear
 521 to be negative (uplift). However, bearings were not designed to accommodate such behavior. Even if the
 522 FE model is modified to include this possibility, it is still not sure that the bilinear behavior is a correct
 523 assumption. For this reason, the engineer decides to start a fourth iteration of the identification framework
 524 with a new model class that includes for the non-linear behavior uncertainty of the bearings as a source of
 525 modeling uncertainty.

526 3.4. Identification framework iteration 4

527 In this fourth iteration, the engineer decides to estimate the uncertainties associated with the non-linear
 528 behavior of the bearings in order to include them in a new model class \mathcal{G}_4 . The error due to the non-linear
 529 behavior is estimated through the comparison of the measured values and a model that behaves linearly with
 530 respect to the loading. Based on the representation of the relationship between measured displacement and
 truck load, coordinates of points A, B and C are known (see Figure 13). The linear model should pass by

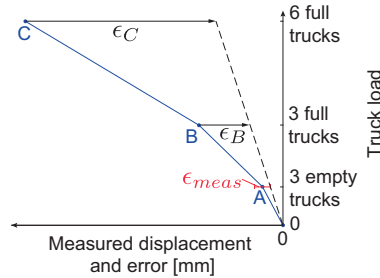


Figure 13: Schematic representation of the estimation of the error associated with the non-linear bridge behavior.

531
 532 the coordinates (0;0) and the point A where the load is caused by the three empty trucks. For this load, the

533 bridge behavior is assumed to be linear. However, since the measured value at point A is associated with a
534 measurement error whose upper bound is 0.25 mm. By adding this upper-bound error value to the measured
535 value in A, a second point is determined in order to draw the linear model that represents the worst case
536 scenario for the error associated with the non-linear behavior. These errors ϵ_B and ϵ_C are then represented
537 by the difference between points B and C and the linear model. These values represent an upper bound
538 for the uncertainty. The lower bound is set to 0 and thus the uncertainty associated with the non-linear
539 behavior \mathbf{W}_{nl} is assumed to follow a uniform PDF with boundaries 0 and either ϵ_B or ϵ_C .

540 With this additional source, the uncertainties associated with model class \mathcal{G}_4 become

$$541 \quad \mathbf{U}_{g_4} = \mathbf{U}_{g_3} + \mathbf{W}_{nl} \quad (14)$$

542 The FE model is modified in order to account for linear behavior of the bearings as it was for model class
543 \mathcal{G}_2 such that $g_4 \equiv g_2$. The parameters $\boldsymbol{\theta}_4 = [\theta_{\text{rot-ext}}, \theta_{\text{rot-int}}, \theta_{\text{conc}}]^\top$ are the rotational stiffness of the exterior
544 bearings, the rotational stiffness of the interior bearings and Young's modulus of concrete. As determined
545 for model class \mathcal{G}_3 , the bearing stiffness of the straight bridge side are included in the uncertainties \mathbf{U}_{g_4} due
546 to their low influence on the displacement responses. Thus, only the stiffnesses of bearings located on the
547 skewed side are parameter values requiring identification.

548 For the next model-falsification step, an initial model set $\Omega_4 = \{\boldsymbol{\Theta}_4\}$ of $n_{\Omega_4} = 1,728$ model instances is
549 generated by dividing the parameter ranges to 11 uniform intervals. Using the $n_y = 48$ measurements of LC-
550 1, 2, 3 and 5 and model predictions $g_4(x_{kl}, \boldsymbol{\Theta}_4)$, x_{kl} with $k \in \{1, 2, \dots, 12\}$ and $l \in \{1, 2, 3, 5\}$, 4 candidate
551 models are identified and more than 98% of the initial population is falsified. Although this means that the
552 model class \mathcal{G}_4 is correct, before making conclusions in the diagnostic step, a study of model-class robustness
553 should be carried out due to the high ratio of rejected models.

554 3.4.1. *Diagnosis robustness*

555 The sensitivity to erroneous measurements is conducted in order to evaluate diagnosis robustness as
556 presented in Section 2.5. Thus, in the first step, $n_y = 47$ measurements corresponding to the removal of a
557 single element in the matrix x_{kl} are compared with model predictions for each model-falsification iteration
558 assuming that only one measurement may be erroneous. In the second step, each measurement is removed
559 one by one for every load case since it is likely that an erroneous measurement remains erroneous during
560 other load cases. Thus, for each falsification iteration, a row is removed from the matrix x_{kl} . During the
561 two processes, the number of candidate models obtained for each iteration is stored and the sensitivity to
562 erroneous measurements can be evaluated through the variation in the number of candidate models.

563 Figure 14 shows the result of both processes for model class \mathcal{G}_4 . When removing individually a single
564 measurement and thus using $n_y = 47$ measurements, the model falsification leads to the same 4 candidate
565 models as found using the set of 48 measurements, except under removal of $x_{2,1}$ and $x_{2,3}$ measurements

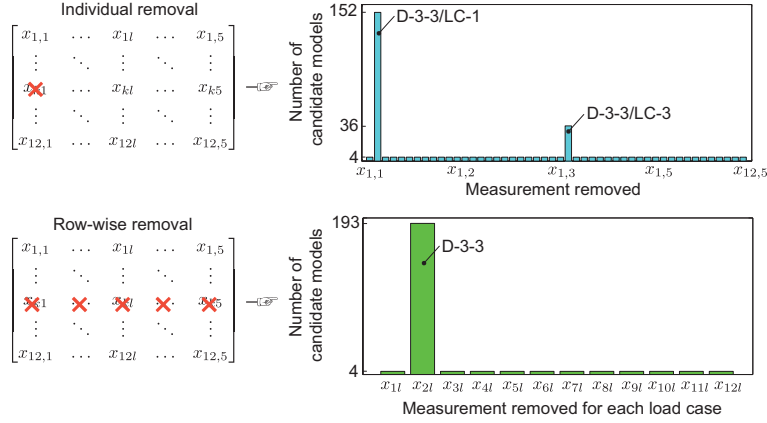


Figure 14: Diagnosis sensitivity to single measurement removal for any load case and for each load case for model class \mathcal{G}_4 .

566 referring to sensor D-3-3 under LC-1 and LC-3. The identification results are sensitive to the removal of
 567 these measurements since the number of candidate models increases to 152 and 36, respectively. In addition,
 568 when removing the measurements for each load case during the model falsification (comparison of $n_y = 44$
 569 measurements), each measurement configuration obtained leads to the same 4 candidate models except when
 570 removing sensor D-3-3 for which the number of candidate models increases to 193.

571 This investigation shows a high sensitivity of the diagnostics to sensor D-3-3, particularly under LC-1
 572 and LC-3. This means that keeping this sensor in the identification process may hide hundreds of possible
 573 solutions. Since the removal of this sensor for two load cases shows diagnostic sensitivity, a robust approach
 574 is the removal of this sensor for each load cases and keeping the identification of 193 candidate models as
 575 the diagnostic result. In addition, the robust set of 193 candidate models includes the 4 candidate models
 576 previously identified.

577 Figure 15 presents a pairwise comparison of the candidate-model parameter values that are identified for
 578 the three parameters. Each axis represents the initial possible values for every parameter. Although this
 579 figure shows that the 193 candidate models do not reveal a significant reduction in the parameter ranges,
 580 it presents a significant reduction in the number of permutations of the interior bearing stiffness values and
 581 concrete Young's modulus values. In addition, the pairwise comparison of exterior and interior bearing
 582 values confirms that they are likely unequal due to the difference of their deterioration state.

583 Note that this sensitivity study is also carried out for model class \mathcal{G}_1 to \mathcal{G}_3 in order to guarantee that
 584 a single measurement is not responsible for the model-class falsification. Each process returns an empty
 585 candidate-model set for any sensor removed ensuring the robustness of the model-class falsification.

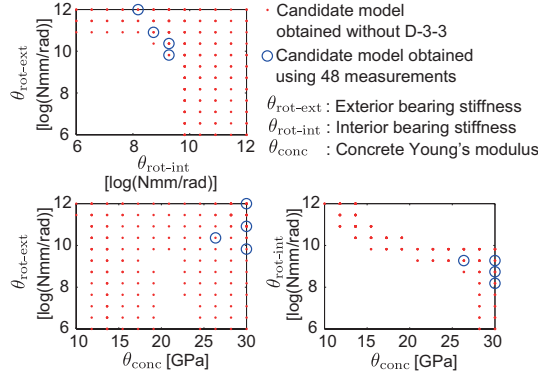


Figure 15: Pairwise comparison of parameter values that are identified using the identification framework.

586 3.4.2. Prognosis and next steps

587 In the next step, since the diagnostics is adequate, the 193 candidate models are used to predict displacement for LC-4 and LC-6 and to verify the diagnostics. To do this, the procedure presented in Section 2.6
 588 is employed with $\phi_p = 0.95$. In Eq. (8), the uncertainty term U_{j,g_κ} is $U_{j,g_4} - U_{j,\hat{y}}$, including the measurement uncertainty, since the prognoses here is compared with measured values. The predicted ranges that
 589 are bounded by the prediction threshold includes the measured value for all locations. Figure 16 presents
 590 a prognosis example for sensor D-1-2 under LC-6 as well as the prognosis that is obtained with the initial
 591 model set (i.e. if structural identification would have not been performed). A high reduction in uncertainty
 592

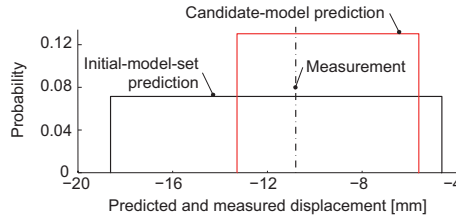














Figure 16: Comparison of prediction distribution and measured value for displacement of sensor D-1-2 under LC-6.

593
 594 is revealed between the initial-model-set and candidate-model-set predictions. However, even after identification the prediction range is large (between -6 and -13 mm). This is due to the modeling uncertainties
 595 that include the non-linear behavior uncertainty which has a high influence, as presented in Table 4.
 596

597 This table shows that the non-linear behavior uncertainty has 25% importance before identification, which is the highest relative importance. However, this uncertainty source cannot be identified as the
 598 parameters θ_4 and cannot be reduced using information provided by measurements. Also, this table depicts
 599 that the parameter relative importance decreases significantly after identification showing the benefits of
 600

Table 4: Relative importances of parameter, modeling and measurement uncertainties for identification framework iteration 4. The relative importance values are averaged over all displacement measurement locations.

Uncertainty source	Relative importance	
	Before identification	After identification
Exterior bearing rotational stiffness	10 % 	5.0 % 
Interior bearing rotational stiffness	23 % 	6.0 % 
Young's modulus of concrete	12 % 	3.0 % 
Modeling uncertainties	17 % 	23 % 
Measurement uncertainties	13 % 	21 % 
Non-linear behavior	25 % 	42 % 

601 structural identification.

602 Note also that using the measurements of all load cases (LC-1 to LC-6), model falsification leads to
 603 the same 4 candidate models obtained using only four load cases. This shows that the four load cases are
 604 sufficient to identify the structural behavior of this bridge.

605 Assuming that a prognosis of the remaining fatigue life is required, it is likely that the prognosis perfor-
 606 mance will be inadequate by extrapolating results from Figure 16. Indeed, the uncertainty associated with
 607 the predictions is too large and the source of uncertainty that is responsible for this is difficult to estimate
 608 for conditions other than those prevailing during monitoring due to the lack of knowledge of the true bearing
 609 device behavior. Two scenarios may be examined in order to guide the engineer in his decision related to
 610 the subsequent steps:

- 611 • Scenario I: Prognosis results are required. The next step should be a new monitoring task focusing on
 612 the bearing-device behavior that will lead to a new diagnostic and a more accurate prognosis.
- 613 • Scenario II: The cause of the non-linear behavior has been identified, and thus intervention is required
 614 to avoid other bridge components from being damaged by such unexpected behavior. The intervention
 615 would be the replacement of the bearing devices on the skewed side since those on the straight side
 616 have shown to have a low influence on the bridge response. Then, further monitoring is required to
 617 identify a new model class in order to carry out a revised prognosis.

618 In such situations, the engineer should compare the costs of both scenarios. Scenario II could be more
 619 appropriate since bearing devices are likely to be replaced as a result of scenario I.

620 **4. Summary and discussion**

621 This example demonstrated that an iterative process is necessary for acquiring important information and
 622 knowledge to perform structural identification. Figure 17 summarizes the iterations and the steps required
 in this case study where arrows illustrate decisions of the engineer. Although the case study of US202/NJ23

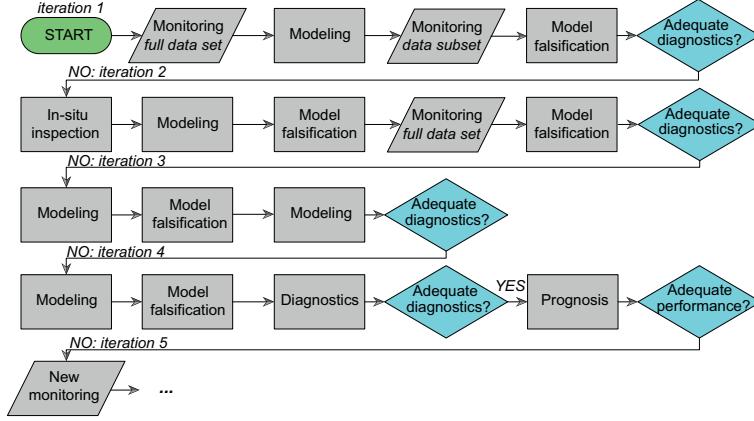


Figure 17: Iterative structural identification process for US202/NJ23 Bridge.

623 Bridge presents a partial structural identification process, it illustrates the process of the engineer acquiring
 624 knowledge to make better decisions regarding structural health management. Indeed, starting with a naive
 625 model class originating from his basic knowledge, the iterative process increased the engineer's knowledge
 626 of the structural behavior to a state at which a decision is possible. As shown in Table 5, each iteration
 627 increases the knowledge acquired either by raw information on the structure or interpreting measurement
 628 data.

Table 5: Summary of the iterative structural identification framework applied to US202/NJ23 Bridge.

Iter.	Model class	Acquired information	Acquired knowledge
1	$\mathcal{G}_1 = \{g_1(\mathbf{x}, \boldsymbol{\theta}_1)\} \cup \{\mathbf{U}_{g_1}\}^a$, $\boldsymbol{\theta}_1 = [\theta_{\text{rot}}, \theta_{\text{conc}}]^T$	$\Omega_1^* = \emptyset$, measurements, drawings	Basic knowledge
2	$\mathcal{G}_2 = \{g_2(\mathbf{x}, \boldsymbol{\theta}_2)\} \cup \{\mathbf{U}_{g_1} + \mathbf{V}_{\text{pier}}\}$, $\boldsymbol{\theta}_2 = [\theta_{\text{rot-ext}}, \theta_{\text{rot-int}}, \theta_{\text{conc}}]^T$	$\Omega_2^* = \emptyset$, deteriorations (inspection)	Pier-cap crack low impor- tance, bearing non-linear behavior
3	$\mathcal{G}_3 = \{g_3(\mathbf{x}, \boldsymbol{\theta}_3)\} \cup \{\mathbf{U}_{g_2} + \sum_{r=1}^8 \mathbf{V}_{\text{rot-r}}\}$, $\boldsymbol{\theta}_3 = [\theta_{\text{rot-1s-C}_1}, \theta_{\text{rot-1s-C}_2}, \theta_{\text{rot-1s-}\phi}, \dots, \theta_{\text{conc}}]^T$	$\Omega_3^* = \emptyset$	Inadequate bilinear behav- ior
4	$\mathcal{G}_4 = \{g_4(\mathbf{x}, \boldsymbol{\theta}_4)\} \cup \{\mathbf{U}_{g_3} + \mathbf{W}_{\text{nl}}\}$, $\boldsymbol{\theta}_4 = [\theta_{\text{rot-ext}}, \theta_{\text{rot-int}}, \theta_{\text{conc}}]^T$	$\Omega_4^* = \{\Theta_4\}$, $n_{\Omega_4^*} = 193$	Complex non-linear behav- ior, inaccurate predictions

^aUncertainties are composed of numbers #3 to #10 of Table 1.

630 In such a process, the falsification perspective and engineering heuristics play the main role, since they
631 help engineers structure their knowledge through discarding wrong hypotheses about the structural behavior.
632 Thus, he could falsify the bilinear behavior model of the bearing and confirm the low influence of the straight-
633 side bearing stiffness. This limits interventions to the skewed-side bearing devices. In addition, the low
634 influence of pier-cap-cracks on bridge behavior is confirmed by identifying the 193 candidate models and
635 thus temporarily rejecting the retrofit of this bridge component.

636 For complex structures, the right physics-based model is never uniquely identified. However, using the
637 structural identification framework, engineers are supported through reasoning with discrete populations
638 of model instances. By testing hypotheses under the form of model classes through the model-falsification
639 task, engineers gain a better understanding of the sources of discrepancies between model predictions and
640 measurements. Such knowledge may be then helpful for increasing accuracy related to the prognosis task.

641 Lack of precise prognosis originates from the fact that given available knowledge, modeling uncertainty is
642 too high. Further investigation is required to reduce this uncertainty. While a calibrated model may always
643 give an answer, it may not result in reliable structural identification and thus may lead to wrong predictions
644 and unnecessary actions, particularly when extrapolating [3, 14].

645 Nevertheless, improvements are necessary in order to increase the robustness of the approach. Indeed,
646 the non-linear behavior is identified only by LC-1 and LC-5 in addition to LC-2 and LC-3. Without the data
647 of these load cases, a wrong model class could have been identified. In addition, the non-linear behavior
648 uncertainty would have been difficult to estimate if the static-load test had not been carried out by step-wise
649 increases in loading. Thus, more effort is required to determine optimal loading strategies.

650 **5. Conclusion**

651 This paper proposes a new iterative structural identification framework for the diagnosis and prognosis of
652 existing structures. A full-scale study involving US202/NJ23 Bridge illustrates the benefits of the framework.
653 This study leads to the following conclusions:

- 654 • This approach is able to support structural identification through combining engineering heuristics
655 with on-site measurements and is robust to modeling systematic uncertainties.
- 656 • The iterative structural identification framework explores the compatibility of several model classes by
657 model-class falsification.
- 658 • The study of the bridge in Wayne shows that the modeling uncertainty is dominated by complex non-
659 linear behavior of the bearing devices, thereby leading to the need for additional monitoring campaign
660 for better identification.

661 Acknowledgements

662 The authors acknowledge the Intelligent Infrastructure Alliance from Drexel University, particularly
663 Prof. A. Emin Aktan, Prof. Franklin L. Moon and Dr. Jeff Weidner, for providing the case study and
664 the measurement data. The authors also thank the International Bridge Study (IBS) Group that was
665 initiated with the Center for Advanced Infrastructure and Transportation (CAIT) of Rutgers University, New
666 Jersey Department of Transportation and Federal Highway Administration Long-Term Bridge Performance
667 Program support and located in Rutgers. The authors also thank Dr. James-A. Goulet for support and
668 fruitful discussions. This work was funded by the Swiss National Science Foundation under Contract no.
669 200020-155972.

670 References

- 671 [1] S. Atamturktur, Z. Liu, H. Cogan, S. and Juang, Calibration of imprecise and inaccurate numerical models considering
672 fidelity and robustness: a multi-objective optimization-based approach, *Structural and Multidisciplinary Optimization*
673 (2014) 1–13.
- 674 [2] J. Beck, Bayesian system identification based on probability logic, *Structural Control and Health Monitoring* 17 (7) (2010)
675 825–847.
- 676 [3] J.-A. Goulet, I. Smith, Structural identification with systematic errors and unknown uncertainty dependencies, *Computers*
677 *& Structures* 128 (2013) 251–258.
- 678 [4] F. Çatbaş, T. Kijewski-Correa, A. Aktan, Structural identification of constructed systems, Reston (VI): American Society
679 of Civil Engineers .
- 680 [5] J. Beck, L. Katafygiotis, Updating models and their uncertainties. I: Bayesian statistical framework, *Journal of Engineering*
681 *Mechanics* 124 (4) (1998) 455–461.
- 682 [6] B. Goller, G. Schuëller, Investigation of model uncertainties in Bayesian structural model updating, *Journal of Sound and*
683 *Vibration* 330 (25) (2011) 6122–6136.
- 684 [7] H. Lam, H. Peng, S. Au, Development of a practical algorithm for Bayesian model updating of a coupled slab system
685 utilizing field test data, *Engineering Structures* 79 (2014) 182–194.
- 686 [8] J. Beck, K.-V. Yuen, Model selection using response measurements: Bayesian probabilistic approach, *Journal of Engineering*
687 *Mechanics* 130 (2) (2004) 192–203.
- 688 [9] K. Worden, J. J. Hensman, Parameter estimation and model selection for a class of hysteretic systems using Bayesian
689 inference, *Mechanical Systems and Signal Processing* 32 (2012) 153–169.
- 690 [10] C. Argyris, P. Tsopelas, C. Papadimitriou, Bayesian Uncertainty Quantification in Seismically Isolated Structures Equipped
691 with Nonlinear Hysteretic Devices, in: J. Rodellar, A. Güemes, F. Pozo (Eds.), *Proceedings of the 6th World Conference*
692 *on Structural Control and Monitoring (WCSCM)*, Barcelona, Spain, 2478–2488, 2014.
- 693 [11] N. Dubbs, F. Moon, Comparison and Implementation of Multiple Model Structural Identification Methods, *Journal of*
694 *Structural Engineering* in press (2015) 04015042.

- 695 [12] B. Goller, J. Beck, G. Schuëller, Evidence-Based Identification of Weighting Factors in Bayesian Model Updating Using
696 Modal Data, *Journal of Engineering Mechanics* 138 (2012) 430–440.
- 697 [13] D. Straub, I. Papaioannou, Bayesian updating with structural reliability methods, *Journal of Engineering Mechanics*
698 141 (3) (2014) 04014134.
- 699 [14] R. Pasquier, I. F. C. Smith, Robust system identification and model predictions in the presence of systematic uncertainty,
700 *Advanced Engineering Informatics* (2015) in press.
- 701 [15] J. Ching, Y.-C. Chen, Transitional Markov chain Monte Carlo method for Bayesian model updating, model class selection,
702 and model averaging, *Journal of Engineering Mechanics* 133 (7) (2007) 816–832.
- 703 [16] M. Muto, J. Beck, Bayesian updating and model class selection for hysteretic structural models using stochastic simulation,
704 *Journal of Vibration and Control* 14 (1-2) (2008) 7–34.
- 705 [17] K.-V. Yuen, *Bayesian methods for structural dynamics and civil engineering*, Wiley, 2010.
- 706 [18] D. Mackay, *Information theory, inference and learning algorithms*, Cambridge University Press, 2003.
- 707 [19] K. Van Buren, T. Hall, L. Gonzales, F. Hemez, S. Anton, A case study to quantify prediction bounds caused by model-form
708 uncertainty of a portal frame, *Mechanical Systems and Signal Processing* 50-51 (2015) 11–26.
- 709 [20] E. Simoen, G. D. Roeck, G. Lombaert, Dealing with uncertainty in model updating for damage assessment: A review,
710 *Mechanical Systems and Signal Processing* 56–57 (2015) 123–149.
- 711 [21] P. Reichert, M. Omlin, On the usefulness of overparameterized ecological models, *Ecological Modelling* 95 (2) (1997)
712 289–299.
- 713 [22] C. Chatfield, Model Uncertainty, *Data Mining and Statistical Inference, Journal of the Royal Statistical Society. Series A*
714 (Statistics in Society) 158 (3) (1995) 419–466.
- 715 [23] E. Simoen, C. Papadimitriou, G. Lombaert, On prediction error correlation in Bayesian model updating, *Journal of Sound*
716 and *Vibration* 332 (18) (2013) 4136–4152.
- 717 [24] H. Choi, K. Beven, Multi-period and multi-criteria model conditioning to reduce prediction uncertainty in an application
718 of TOPMODEL within the GLUE framework, *Journal of Hydrology* 332 (34) (2007) 316–336.
- 719 [25] K. Beven, A. Binley, The future of distributed models: Model calibration and uncertainty prediction, *Hydrological Processes*
720 6 (3) (1992) 279–298.
- 721 [26] M. Beck, Water quality modeling: a review of the analysis of uncertainty, *Water Resources Research* 23 (8) (1987) 1393–
722 1442.
- 723 [27] N. Cherpeau, G. Caumon, J. Caers, B. Lévy, Method for Stochastic Inverse Modeling of Fault Geometry and Connectivity
724 Using Flow Data, *Mathematical Geosciences* (2012) 1–22.
- 725 [28] M. Yarnold, F. Moon, A. Aktan, Temperature-Based Structural Identification of Long-Span Bridges, *Journal of Structural*
726 *Engineering* in press (2015) 04015027.
- 727 [29] M. Fontan, D. Breyse, F. Bos, A hierarchy of sources of errors influencing the quality of identification of unknown
728 parameters using a meta-heuristic algorithm, *Computers & Structures* 139 (2014) 1–17.

- 729 [30] J. Baroth, Y. Malecot, Probabilistic analysis of the inverse analysis of an excavation problem, *Computers and Geotechnics*
730 37 (3) (2010) 391–398.
- 731 [31] H. Schlune, M. Plos, K. Gylltoft, Improved bridge evaluation through finite element model updating using static and
732 dynamic measurements, *Engineering Structures* 31 (7) (2009) 1477–1485.
- 733 [32] F. Moon, A. Aktan, Impacts of epistemic (bias) uncertainty on structural identification of constructed (civil) systems,
734 *Shock and Vibration Digest* 38 (5) (2006) 399–422.
- 735 [33] A. Jakeman, R. Letcher, J. Norton, Ten iterative steps in development and evaluation of environmental models, *Environ-*
736 *mental Modelling & Software* 21 (5) (2006) 602–614.
- 737 [34] A. Aamodt, A case-based answer to some problems of knowledge-based systems, in: *Scandinavian Conference on Artificial*
738 *Intelligence-93: Proceedings of the Fourth Scandinavian Conference on Artificial Intelligence Electrum, Stockholm, Sweden,*
739 *May 4-7, 1993, vol. 18, IOS Press, 168, 1993.*
- 740 [35] K. Popper, *The logic of scientific discovery*, 3rd ed. New York, Routledge, 2002.
- 741 [36] A. Tarantola, Popper, Bayes and the inverse problem, *Nature Physics* 2 (8) (2006) 492–494.
- 742 [37] K. Beven, A manifesto for the equifinality thesis, *Journal of Hydrology* 320 (1-2) (2006) 18–36.
- 743 [38] R. Pasquier, I. Smith, Sources and forms of modelling uncertainties for structural identification, in: *Proceedings of 7th*
744 *International Conference on Structural Health Monitoring of Intelligent Infrastructure (SHMII), Torino, IT, 2015.*
- 745 [39] S. Atamturktur, F. Hemez, J. Laman, Uncertainty quantification in model verification and validation as applied to large
746 scale historic masonry monuments, *Engineering Structures* 43 (2012) 221–234.
- 747 [40] K. Van Buren, M. Mollineaux, F. Hemez, S. Atamturktur, Simulating the dynamics of wind turbine blades: part II, model
748 validation and uncertainty quantification, *Wind Energy* 16 (5) (2013) 741–758.
- 749 [41] J.-A. Goulet, C. Michel, I. Smith, Hybrid probabilities and error-domain structural identification using ambient vibration
750 monitoring, *Mechanical Systems and Signal Processing* 37 (1-2) (2013) 199–212.
- 751 [42] J.-A. Goulet, M. Texier, C. Michel, I. Smith, L. Chouinard, Quantifying the Effects of Modeling Simplifications for
752 Structural Identification of Bridges, *Journal of Bridge Engineering* 19 (1) (2014) 59–71.
- 753 [43] R. Pasquier, J.-A. Goulet, C. Acevedo, I. Smith, Improving Fatigue Evaluations of Structures Using In-service Behavior
754 Measurement Data, *Journal of Bridge Engineering* 19 (11) (2014) 04014045.
- 755 [44] J.-A. Goulet, I. Smith, Performance-Driven Measurement System Design for Structural Identification, *Journal of Comput-*
756 *ing in Civil Engineering* 27 (4) (2013) 427–436.
- 757 [45] R. Pasquier, J.-A. Goulet, I. Smith, Model-Based Data Interpretation and Diagnosis Robustness, in: Deodatis, Ellingwood,
758 Frangopol (Eds.), *Safety, Reliability, Risk and Life-Cycle Performance of Structures & Infrastructures. Proceedings of 11th*
759 *International Conference on Structural Safety & Reliability (ICOSSAR), New York, USA, 2497–2504, 2014.*
- 760 [46] M. Papadopoulou, B. Raphael, I. Smith, C. Sekhar, Hierarchical Sensor Placement Using Joint Entropy and the Effect of
761 Modeling Error, *Entropy* 16 (9) (2014) 5078–5101.

